Spectrum Sensing Everywhere: Wide-Band Spectrum Sensing With Low-Cost UWB Nodes

Zhicheng Luo, Qianyi Huang, *Member, IEEE*, Xu Chen, *Senior Member, IEEE*, Rui Wang, *Member, IEEE*, Fan Wu, *Member, IEEE*, Guihai Chen, *Fellow, IEEE*, and Qian Zhang, *Fellow, IEEE*

***Abstract*— Spectrum sensing plays a crucial role in spectrum monitoring and management. However, due to the expensive cost of high-speed ADCs, wideband spectrum sensing is a long-standing challenge. In this paper, we present how to transform Ultra-wideband (UWB) devices into a spectrum sensor which can provide wideband spectrum monitoring at a low cost. Compared with the expensive high-speed ADCs which cost at least hundreds of dollars, a UWB device is only several dollars. As the low-cost UWB technology is not originally designed for spectrum sensing, we address the inherent limitations of low-cost devices such as limited memory, low SPI speed and low accuracy, and show how to obtain spectrum occupancy information from the noisy and spurious UWB channel impulse response. In this paper, we present *WISE*, which not only can give accurate channel occupancy information, but also can precisely estimate the signal power and bandwidth. *WISE* can also detect fleeting radar signals. We implement *WISE* and perform extensive evaluations with both controlled experiments and field tests. Results show that *WISE* can sense up to 900MHz bandwidth with frequency range from 0.5GHz to 7GHz, and the power estimation error is less than 3dB. *WISE* can also accurately detect busy 5G channels and can classify the encrypted traffic from the channel usage patterns. We believe that *WISE* provides a new paradigm for low-cost wideband spectrum sensing, which is critical for large-scale fine-grained spectrum monitoring.**

***Index Terms*— Spectrum sensing, UWB, low-cost, wideband.**

I. Introduction

With the unprecedented amount of wireless traffic and rapidly increasing number of untethered devices, the limited spectrum has been recognized as a scarce, valuable resource. The key to addressing the spectrum scarcity issue is to have a better understanding of the spectrum usage pattern, that is, global information about which channel is occupied/available in both spatial and temporal domains. Thus, city-level fine-grained spectrum monitoring is of vital importance to help regulators make strategic allocations. It is also the key to the success of dynamic spectrum access, where the spectrum is shared among multiple radio access technologies (RATs). For example, in the US, Wi-Fi 6E and 5G New Radio Unlicensed (NR-U) will share the unlicensed 6GHz band [1], where the whole bandwidth is 1200MHz ($5925-7125$MHz); LTE/5G and military radar are sharing the 150MHz CBRS band at 3.5GHz [2].

However, wideband spectrum sensing has been a long-standing challenge. As we know, wideband spectrum sensing requires high-speed ADCs, which are too expensive to be widely affordable. Prior works have proposed several solutions [3], [4], [5], [6], where a low-speed ADC scans a portion of the spectrum each time and stitches the results to generate a wideband spectrum map. Such design principles naturally lead to the drawback that transient signals (e.g., radar) can be easily missed. Researchers also combine software-defined radios with signal processing techniques (e.g., sparse Fourier transform [7], [8], [9]) and advanced scanning strategies [4], [5], [6] to provide wideband spectrum sensing. Unfortunately, they are feasible only when the spectrum is sparsely occupied, which is not always true given the ever-increasing demand for spectrum. S^3 enables sub-Nyquist rate sampling by designing spike-train like filters [10]. However, such customized hardware is not ready for mass production.

We ask the question that, can we enable wideband spectrum monitoring with low-cost, commercial off-the-shelf devices? We have an interesting observation that Ultra-wideband (UWB) technology has the potential to achieve this goal. UWB has a large bandwidth (up to 1GHz), which is originally intended for high-resolution ranging. The time-of-flight (ToF) information is derived from the channel impulse response (CIR). The key point is that the CIRs not only present the channel information between the UWB TX and RX pair, but also record all in-band ongoing transmission in the air. It brings the feasibility that we can obtain wideband channel information from UWB receivers. UWB technology has already been integrated into commercial products, such as smartphones (e.g., iPhone 14/15 [11], [12], Galaxy Note 20 Ultra [13], and Xiaomi MIX 4 [14]) and IoT devices (e.g., Air tag [15], Apple watch [16] and Samsung Galaxy

Manuscript received 2 June 2023; revised 11 October 2023; accepted 20 November 2023; approved by IEEE/ACM TRANSACTIONS ON NETWORKING Editor C. Peng. This work was supported in part by the Key-Area Research and Development Program of Guangdong Province under Grant 2020B0101390001; in part by the National Natural Science Foundation of China under Grant 62002150; and in part by the Research Grants Council under Contract Competitive Earmarked Research Grant 16204820, Contract 16206122, Contract AoE/E-601/22-R, Contract R8015, and Contract 3030_006. *(Corresponding author: Qianyi Huang.)*

Zhicheng Luo is with the School of Computer Science and Engineering, Sun Yat-sen University, Guangzhou 510006, China, and also with the Peng Cheng Laboratory, Shenzhen 518000, China (e-mail: luozhch23@mail2.sysu.edu.cn).

Qianyi Huang and Xu Chen are with the School of Computer Science and Engineering, Sun Yat-sen University, Guangzhou 510006, China (e-mail: huangqy89@mail.sysu.edu.cn; chenxu35@mail.sysu.edu.cn).

Rui Wang is with the Department of Electrical and Electronic Engineering, Southern University of Science and Technology, Shenzhen 518055, China (e-mail: wang.r@sustech.edu.cn).

Fan Wu and Guihai Chen are with the Department of Computer Science and Engineering, Shanghai Jiao Tong University, Shanghai 200240, China (e-mail: fwu@cs.sjtu.edu.cn; gchen@cs.sjtu.edu.cn).

Qian Zhang is with the Department of Computer Science and Engineering, The Hong Kong University of Science and Technology, Hong Kong (e-mail: qianzh@cse.ust.hk).

Digital Object Identifier 10.1109/TNET.2023.3342977

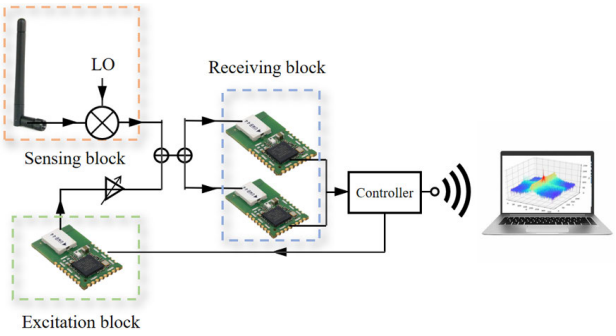

Fig. 1. System overview of *WISE*.

SmartTag+ [17]), which indicates that these daily devices may be turned into a spectrum sensor that facilitates the large-scale spectrum sensing.

In this paper, we present *WISE*, a low-cost WIdeband Spectrum sEnsing unit. As Figure 1 shows, in *WISE*, there is an excitation block, a receiving block, and a sensing antenna. The excitation block transmits UWB packets continuously to trigger the receiving block. These UWB packets and in-air signals from the sensing antenna are combined and then fed into the receiving block. CIRs are extracted from the receiving block, from which we can derive the frequency and bandwidth of the in-air signals. Although the idea sounds straightforward, it is not trivial to achieve the goal. Since the low-cost UWB devices can not afford high-speed clocks and ADCs to support high sampling rates and high data transfer rates, they show some inherent limitations, including low SPI speed and low accuracy. To make things complicated, it is hard to predict the power level of external signals. We attempt to overcome these challenges as follows:

Low accuracy. A spectrum sensor with UWB chips needs to provide accurate and reliable sensing results. However, due to the low-cost nature of UWB technology, we can hardly ensure that the hardware returns reliable results. Since these chips are proprietary technology, we do not have access to the internal designs. Thus, it is hard to analyze their working mechanism but can only observe their responses to external stimuli. From our experiments, we observe that DW1000, a popular UWB chip on the market, may return noisy CIRs which can lead to poor sensitivity and false positives for channel occupation. Even for the same stimulus, two DW1000 chips will return different CIRs, each with some spurious energy at random frequencies. To address this challenge, we design a mechanism to extract in-air signals from the noisy UWB CIRs, separating external in-air signals from internal UWB signals. To handle the spurious and random frequency response, in *WISE*, we utilize two UWB receivers and let them work in parallel. Since the two chips are unlikely to generate the same spurious frequency response, by taking the intersections from the two receivers, spurious frequency responses can be eliminated.

Low SPI speed. Limited by the SPI speed (20Mbps at maximum), it takes almost 2ms to fetch one CIR sample (1016 points) from the UWB device, i.e., DW1000. *WISE* will miss fleeting signals, such as radar signals, that appear when the chip is performing SPI communication. To address this challenge, instead of getting a complete CIR sample, *WISE* will just get a portion of the CIR. This will reduce the time required for SPI communication but comes at the sacrifice of frequency resolution. We design a mechanism to detect channel occupancy with incomplete CIR samples. We also carefully decide the inter-packet time interval so that *WISE* has a high probability to detect radar signals.

Non-predictable signal power. When a high power base station or Access Point is in close proximity, strong external signals may overwhelm the internal UWB communication, resulting in the receiver failing to detect UWB packets and no CIRs will be available. To make things worse, as the UWB receiver has an automatic gain control unit, it will automatically adjust the receiver gain, which results in uncontrollable scaling of the received signals and makes it hard to estimate the signal power. To address this challenge, *WISE* will dynamically adjust the internal transmission power according to the UWB packet reception ratio. When *WISE* suffers high packet loss, it is possibly due to low SINR. Thus, *WISE* will increase the TX power so that the receiving block has sufficient SINRs to detect UWB packets. As the transmission power of the internal UWB packets is a known system parameter, *WISE* utilizes it as a benchmark to derive the instantaneous AGC gain, and then estimate the actual power of the external signals.

Limited frequency range. As the FCC has authorized the unlicensed use of UWB in the frequency range from 3.1 to 10.6 GHz, most of UWB chips have a limited frequency range. For example, the UWB chip DW1000 supports six bands from 3.1GHz to 7GHz which covers the 3.5GHz CBRS band (coexistence of LTE and military radar) and the unlicensed 6GHz band (coexistence of Wi-Fi 6E and 5G). However, at present, many signals we used in our daily lives are allocated in 2-3GHz, such as Wi-Fi signals and 4G signals. These signals are worth observing and studying, while *WISE* would miss them as they are outside the limited frequency range of UWB. To address this challenge, we can add a frequency translator to convert these signals into the frequency range of the UWB chip. In this way, we can enable *WISE* to support a larger frequency range from 500MHz to 7GHz.

In this paper, we design *WISE*, which is a low-cost wideband spectrum sensor that has high sensing accuracy, good receiver sensitivity, and a wide dynamic range. Different from existing low-cost spectrum sensors [3], [18], [19], [20], *WISE* can sense a wide bandwidth with one single detection. *WISE* is implemented with DW1000 UWB chips, which has the maximum receiver bandwidth about 900MHz [21]. *WISE* can detect weak signals down to -85dBm/MHz and has a dynamic range about 60dB. The power estimation error is 3dB. It can also detect transient or fleeting signals like radar. Besides, *WISE* has good ability to detect 5G signals and can accurately estimate the power of 5G signals at different distances and in complex environments. Based on the spectrum usage patterns of the user's smartphones, WISE can infer what category of applications the users are using, such as watching a video, playing games, or downloading files. The total cost of *WISE* is about 20 dollars, making it possible to be widely deployed and used for various purposes including 5G base station maintenance, 5G signal propagation research, city-level

spectrum planning or interference source localization. As the limitations of DW1000 are generic among UWB devices, the design principles of *WISE* can extend well to other devices.

In this paper, we make the following major contributions:

- We demonstrate the spectrum sensing capability of UWB chips, which provides a new direction to build cheap and wideband spectrum sensors.
- We design *WISE*, a low-cost spectrum sensor that supports up to 900MHz bandwidth with high accuracy, good sensitivity, and wide dynamic range. *WISE* can also detect fleeting radar signals.
- We extensively evaluate the performance of *WISE*. From the results, we can see that *WISE* can achieve good accuracy in busy channel detection and signal power estimation. We also show that *WISE* can detect busy 5G channels and accurately estimate 5G signal power.

The remainder of this paper is organized as follows. In Section II, we introduce UWB technology and the rationale why UWB can be used for spectrum sensing. We present the system overview in Section III and system design details are illustrated in Section IV. In Sextion V, we show a case study of *WISE* to classify some encrypted Internet traffic. Implementation details are described in Section VI and evaluation results are present in Section VII. We review related works in Section VIII and discuss remaining issues in Section IX. Finally, we conclude this work in Section X.

II. Spectrum Sensing Capability of UWB

In this section, we explore the spectrum sensing capability of UWB. We first introduce the UWB technology and then illustrate why it can provide the spectrum sensing function. Following that, we illustrate the system requirements for such a low-cost wideband spectrum sensor.

A. Ultra-Wideband Technology

Ultra-wideband (UWB) technology transmits signals over a wide bandwidth ($>$ 500 MHz). According to the Federal Communications Commission (FCC), the frequency range of UWB is from 3.1 to 10.6 GHz, and the power spectral density (PSD) limit is -41.3dBm/MHz. Typical applications of UWB include ranging and indoor localization. UWB can track assets at a precision of 10 cm, which is a big advantage over Wi-Fi and Bluetooth. Recently, UWB has been integrated into many commercial devices for positioning, tracking, and sensing. For example, Apple's latest iPhones have enabled UWB technology and Apple also released the UWB-equipped asset tracking gadget, AirTag. Samsung has also launched UWB-enabled smartphones and SmartTag+, which is similar to AirTag.

The key that UWB can achieve high ranging resolution is that it can obtain high-precision timestamps. According to IEEE 802.15.4-2011 standard [22], the LSB of the ranging counter value shall represent $1/128$ of a chip time at the mandatory chipping rate of 499.2 MHz, that is, 63.897GHz. DW1000, a popular UWB chip on the market, can provide a time resolution of 15.65 picoseconds.

Fig. 2. Frame format for UWB packets (from [21]).

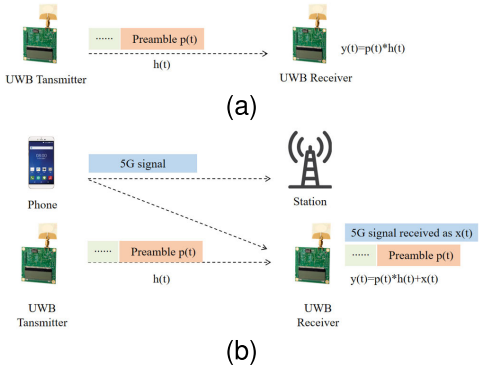

Fig. 3. UWB communication with/without in-air signals. (a) UWB communication. (b) UWB communication with 5G signal.

The frame format of a UWB packet is shown in Figure 2. There is a preamble field, followed by the start of frame delimiter (SFD), PHY header (PHR) and the payload. The UWB TX will record the timestamp when the first symbol of the PHR is transmitted, and accordingly, the RX will record the timestamp when the first symbol of the PHR is received. In this way, time-of-flight (ToF) can be calculated. For the rest of the paper, we will describe our system based on DW1000, a popular UWB chip from Decawave, which has been acquired by Qorvo.

The preamble sequence has a property of perfect periodic autocorrelation, which allows a coherent receiver to determine the exact impulse response of the RF channel between transmitter and receiver [21], [23]. DW1000 provides access to the channel impulse response (CIR) data. For each tap of the CIR, it is a complex value, with a 16-bit real integer and a 16-bit imaginary integer. Each tap represents a 1 ns sample interval. To be more precise, it is half a period of the 499.2 MHz fundamental frequency. For simplicity, we say that the sampling frequency is 1 GHz.

B. UWB for Spectrum Sensing

Assume that there is only a UWB TX and a UWB RX in the system, as shown in Figure 3(a). When the TX transmits the preamble sequence $p(t)$, the RX will receive

$$y(t) = p(t) * h(t),$$

where $h(t)$ is the channel impulse response (CIR) between the TX and RX, and $*$ denotes convolution. To obtain CIR, the RX performs decorrelation of the received signal $y(t)$ with the known preamble sequence.

When there are other transmitters in the air, as shown in Figure 3(b), we denote the superimposed signals arriving at RX's antenna by $x(t)$. Though there are still wires connecting the antenna and receiving block, the wire channel response has minimal effect on the frequency and bandwidth of $x(t)$, thus its influence can be considered as negligible. In this case, the RX receives

$$y(t) = p(t) * h(t) + x(t).$$

In this case, the CIR turns out to be:

$$\hat{h}(t) = p(-t) * y(t) = h(t) + p(-t) * x(t). \quad (1)$$

The RX stores $\hat{h}(t)$ in the CIR memory of DW1000. We note that $\hat{h}(t)$ not only contains the information about $h(t)$, but also the other in-band signals in the air. Transforming Eq. (1) into the frequency domain, it becomes

$$\hat{H}(f) = H(f) + P(f) \cdot X(f). \quad (2)$$

$X(f)$ is the frequency domain representation of the in-air signals, which shows the working frequency and bandwidth of the non-UWB transmitters. $P(f)$ is the frequency domain representation of the preamble sequence.

When the channel between UWB TX and RX is stable, we can consider $H(f)$ as a known constant. Furthermore, according to the measurement result in [24], the UWB signals have a flat frequency response for the whole band (i.e., 500MHz), so we have $|P(f)| \approx c$, where c is a constant. Thus, $\hat{H}(f)$ contains the spectrum usage information, i.e., which frequency bands are occupied and which bands are idle. It indicates that we can use UWB chips for spectrum sensing. Since the bandwidth of UWB is up to 900MHz, we can use the low-cost UWB chip to achieve wideband spectrum sensing. The frequency range of UWB ranges from 3.1GHz to 10.6 GHz, which covers the 3.5 GHz CBRS band and 6GHz unlicensed band. Thus, *WISE* can serve as a spectrum sensor for dynamic spectrum access in these bands.

Here we show some illustrative experiment results. We set up a USRP next to the UWB transceivers to transmit single-tone signals at 3.964GHz. We read CIR samples from DW1000 and perform FFT on the samples to get the channel frequency response (CFR). As the CIR sampling interval is 1ns and there are 1016 samples in total, the frequency resolution of the FFT bins is roughly 1MHz. Figure 7(a) shows the CFR when the USRP is not transmitting and Figure 7(b) shows the CFR when the USRP is transmitting. From Figure 7(b), we can see that the CFR has high peaks around 3.964GHz, which indicates that the UWB captures the single-tone signal transmitted by the USRP. This demonstrates the feasibility of using UWB for spectrum sensing.

C. System Requirements

As UWB is low-cost and wideband by nature, when using it as a spectrum sensor, it needs to meet the following performance requirements:

- High accuracy: It should provide reliable results for channel occupancy detection, with low false positive rate and low false negative rate for the entire band; it should also provide accurate estimations of the signal power.
- Good sensitivity: First, it should be able to detect weak signals. We expect that *WISE* should have the same sensitivity as a typical software-defined radio, e.g., USRP. Second, it should be able to detect short transient packets and fleeting signals, such as radar signals in CBRS band.
- Wide dynamic range: It reflects the ability of *WISE* to detect both high-power and low-power signals. It should be able to detect both strong and weak signals.

In the following sections, we will describe how we design *WISE* to meet these requirements.

III. *WISE* Overview

In this section, we first present the system structure and then give the signal processing flow of *WISE*. As shown in Figure 1, *WISE* has four main components, the sensing block, the excitation block, the receiving block and the controller. The sensing block consists of a sensing antenna and a frequency translator. The sensing antenna is used for picking up ongoing transmissions in the air and the frequency translator is used to translate the frequency of the receiving signals to the UWB frequency. The excitation block is a UWB transmitter, which is responsible for transmitting UWB packets continuously. These packets serve as excitation signals to trigger the receiving block. The receiving block consists of UWB receivers, which are responsible for retrieving the CIRs. A combiner combines the sensing signals and excitation signals, and the output from the combiner is fed to the receiving block via a cable. This is to guarantee that the channel between the UWB TX and RX is as stable as possible. Note that the signals from the excitation block are not emitted into the air, so its continuous transmission will not cause long-lasting interference. The controller is responsible for TX power control, LO selection, working mode selection and CIR processing.

Figure 4 shows the signal processing flow in *WISE*. After LO frequency has been decided by the controller, *WISE* begins receiving the in-air signals. Data processing is mainly performed at the receiving block and it supports two working modes. In normal mode, the first step is to extract in-air signals from noisy CFRs. It is essential to separate the internal UWB signals and in-air signals, which greatly reduces noise level and improves the system sensitivity. The second step is to estimate the power of signals. *WISE* uses the internal signal as the benchmark to estimate the instantaneous AGC gain and then estimates the power of external signals. Then, we use a dynamic threshold to classify busy/idle channels. The signal processing flow in radar mode is similar, but differs in the way that we perform in-air signal extraction and power estimation. The details can be found in Section IV.

IV. *WISE* Design

In this section, we present the design details for each component in *WISE*.

A. Sensing Block

The Sensing block consists of an antenna and a mixer with its local oscillator (LO). The mixer is used to modulate the desired signal to the UWB band. For example, if one wants to observe the Wi-Fi signal in 2.4GHz that is outside the UWB range, *WISE* will set the LO frequency of mixer to 1GHz, and modulate the receiving Wi-Fi signal to 3.4GHz. Then *WISE* can capture the Wi-Fi signal in UWB channel 4 (3.5436GHz-4.4436GHz). However, the addition of the mixer will produce many resonances, which are integral multiples of the LO frequency. For example, when using a USRP X310 to generate a LO signal of 1GHz, there will be other resonances

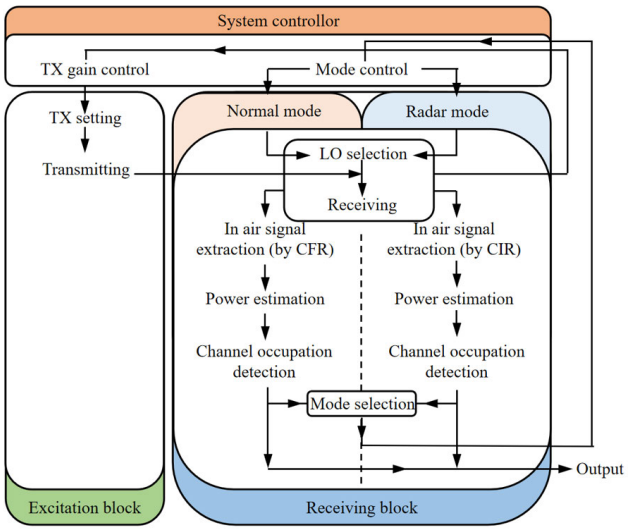

Fig. 4. Signal processing flow in *WISE*.

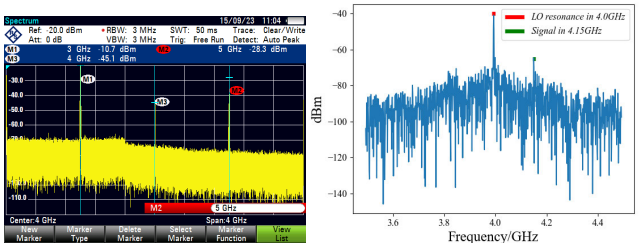

Fig. 5. LO resonances. (a) LO resonances of USRP X310. (b) CFR with LO resonances.

TABLE I
LO-CHANNEL MAPPING TABLE

Frequncy range	LO frequency	UWB frequency range
0.5GHz-1.5GHz	5.5GHz(+0.05GHz)	6.05GHz-6.95GHz
1.5GHz-2.5GHz	4.5GHz(+0.05GHz)	6.05GHz-6.95GHz
2.5GHz-3.25GHz	3.6GHz	6.05GHz-6.95GHz
3.25GHz-4.75GHz	NULL	3.25GHz-4.75GHz
4.75GHz-5.15GHz	1.8GHz	6.05GHz-6.95GHz
5.15GHz- 6GHz	1GHz	6.05GHz-6.95GHz

in 2GHz, 3GHz, and 4GHz…, as shown in Figure 5(a). The resonances may arise from the nonlinearity of circuits [25], [26] and are hard to eliminate in low-cost devices. If the LO resonances appear in the UWB range, those resonances may overwhelm the external signals as shown in Figure 5(b).

To avoid the undesirable harmonics, we design a LO selection method to find a LO frequency that can avoid resonances appearing in UWB frequency range. For that, the LO frequency f_{LO} needs to meet the following conditions:

- $(f^d_{min} + f_{LO}, f^d_{max} + f_{LO}) \in (f^{wi}_{min}, f^{wi}_{max})$
- $k \cdot f_{LO} \notin (f^{wi}_{min}, f^{wi}_{max}), \quad k \in (0, 1, 2, 3 \ldots)$

where (f^d_{min}, f^d_{max}) is the frequency range desired to be observed, and $(f^{wi}_{min}, f^{wi}_{max})$ is UWB frequency range in the i-th channel.

In order to find the appropriate LO frequency that meets the above conditions, we design the following Algorithm 1.

However, it sometime happens that there will be no appropriate LO frequency for f^d_{min} and f^d_{max} when the frequency range covers a wide span (over 500MHz) and is close to the UWB sensing frequency range (3.25GHz-4.75GHz and 6.05GHz-6.95GHz). For that, we design an LO-channel mapping table to cover the whole range from 500MHz to 7GHz with the least LO switches, then we can select the appropriate LO-frequency and UWB channel combination to cover the whole desired frequency range. In our implementation, *WISE* can scan a large bandwidth from 500MHz to 7GHz.

Algorithm 1 LO Selection Algorithm

INPUT f^d_{min}, f^d_{max}
OUTPUT Channel, LOfrequency
$LO_{app} = 0$
for i in range(1,8) **do**
  LO_{min} = min(f^{wi}_{min}-f^d_{min}), (f^{wi}_{max} -f^d_{max}))
  LO_{max} = max((f^{wi}_{min}-f^d_{min}), (f^{wi}_{max} -f^d_{max}))
  for f in range(LO_{min},LO_{max}) **do**
    k = 0, State = 0
    while $k \cdot f < f^{wi}_{max}$ **do**
      if $f^{wi}_{min} < k \cdot f$ **then**
        State = 1
        break
      end if
      k = k+1
    end while
    if State==0 **then**
      Channel = i, LOfrequency = f, $LO_{app} = 1$
      return Channel, LOfrequency
    end if
  end for
end for
if $LO_{app} == 0$ **then**
  Refer to LO-channel mapping table that is shown in Table I
end if

B. Excitation Block

The excitation block is a UWB transmitter, which is intended to trigger the receiving block. According to the user manual of DW1000 [21], once the preamble sequence is detected, the receiver will begin accumulating correlated preamble symbols. Thus, the excitation block transmits UWB packets continuously, which will trigger the receiving block to get constantly updated CIRs. In *WISE* we use UWB transceivers just for obtaining CIRs, not for data communications. Thus, we put only 1 byte data in the payload to make the packets as short as possible.

In order to make sure that the preamble signal can be detected by receivers so as to trigger spectrum sensing, the excitation block needs to dynamically adjust the transmission power to avoid the UWB preamble being buried in strong external signals or being too strong to bury the external signals. Besides, we hope *WISE* can have good sensitivity and wide dynamic range. In *WISE*, we adopt the following control strategy. In the excitation block, we switch the TX power level between two states. By default, the excitation block will transmit at a low power level (State 1). When no UWB packets are detected by the receiving block for a certain time interval,

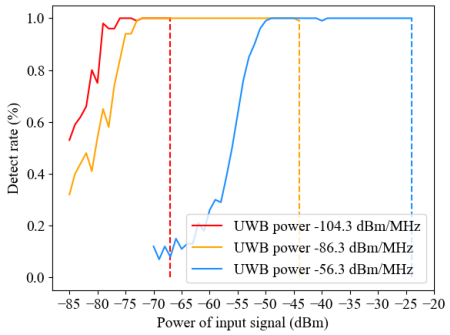

Fig. 6. CFRs under different transmission power.

which is possibly due to low SINR, the receiving block will raise a timeout event. In this case, *WISE* will increase the transmission power of the excitation block (State 2). When the high-power external signal vanishes, *WISE* will switch the TX power to the default low level (State 1).

In order to determine these two power levels, we first use an attenuator to tune the power level of the excitation block. The results are shown in Figure 6. We can see when with a weak preamble power (i.e., -104.3 dBm/MHz), the channel impulse response is very noisy, which makes it hard to extract in-air signal and results in a narrow sensing range. Therefore, we attempt to increase the preamble power. When the power level comes to -86.3 dBm/MHz, *WISE* has the widest sensing range and also has good sensitivity. Thus, we set the power level to be -86.3 dBm/MHz in State 1. As DW1000 can adjust the transmission power around 30 dB and we want to have a wide dynamic range, we set the power level to be -56.3 dBm/MHz in State 2.

Through testing, we find that *WISE* have around 30dB dynamic range in one state. That is, it can detect signals from -85dBm/MHz to -54 dBm/MHz in State 1, and in State 2, it can detect signals with power from -60dBm/MHz to -34dBm/MHz. The whole dynamic range is -85 dBm/MHz ~ -34dBm/MHz.

C. Receiving Block

Before introducing the design details of receiving block, we first present how UWB chips estimate channel impulse response, which will help readers understand the design rationale of *WISE*.

1) CIRs From UWB: According to IEEE standard, each preamble symbol is about 1us and the number of symbols in the preamble can range from 64 to 4096. DW1000 obtains CIR by cross-correlating the received signals with the predefined preamble sequence. The accumulation results are stored in a buffer, named accumulator. Accumulation stops when detecting SFD, while it may stop earlier if the accumulator grows quickly. After saturation, channel impulse response, i.e., the accumulation results, could be read from the accumulator buffer.

As the values we get from the accumulator buffer are the CIR, to analyze the frequency response, we perform FFT on the CIR to get the CFR.

2) In-Air Signal Extraction: According to Equation (2), the CFR we obtained is actually $\hat{H}(f)$, while the spectrum occupation information is contained in $X(f)$. $H(f)$ is the channel response corresponding to the wired channel between UWB TX and RX, which is supposed to be stable. Figure 7(a) shows the CFR when there is no external signal. As long as *WISE* is set up, we can consider $H(f)$ to be constant. During initialization, *WISE* will turn off the RF antenna, where there are only internal UWB signals via the wired cable. *WISE* can obtain $H(f)$ under this circumstance and use it for the following signal extraction procedure. Thus, we can measure $H(f)$ as a system parameter and subtract it from $\hat{H}(f)$. $P(f)$ is the frequency response of the preamble sequence. As defined in IEEE 802.15.4-2011, the preamble is a sequence of short pulses. From the measurement results in [24], we can see that UWB signals have a flat frequency response for the whole band. Thus, we have $|P(f)| \approx c$, where c depends on the transmission power of the excitation block and is also a known system parameter.

However, we can not directly apply Equation (2) to estimate $X(f)$. This is because DW1000 has an automatic gain control (AGC) unit. The AGC will dynamically adjust the receiver gain to ensure optimal receiver performance. Assume that the actual amplitude for frequency f is a_f while the amplitude of frequency f in the FFT results is A_f, then the receiving amplitude $A_f = ka_f$, where k is an unknown coefficient. So the $\hat{H}(f)$ is actually described by Equation (3):

$$\hat{H}(f) = k \cdot [H(f) + P(f) \cdot X(f)]\,. \tag{3}$$

Therefore, we need to figure out k before estimating $X(f)$.

We use a signal generator to transmit 50MHz and 300MHz signals and the corresponding CFRs are shown in Figure 8. Comparing with Figure 7(a), where there is no in-air signals and thus only the $k \cdot H(f)$ component, the $P(f) \cdot X(f)$ term has more spikes in the frequency domain. Thus, we can use a low-degree polynomial to fit the more smooth $k \cdot H(f)$ part, shown as the red curve in Figure 8. We apply a 16-order polynomial curve-fitting on $\hat{H}(f)$. We denote the fitting results by $F(f)$, which is mainly dominated by $k \cdot H(f)$. As we mentioned above, $H(f)$ is a known system parameter. Then, we model it as an optimization problem to determine the scaling factor k as follows:

$$k = \arg\min_{\alpha} \sum_{f=f_{\min}}^{f_{\max}} [F(f) - \alpha \cdot H(f)]^2\,. \tag{4}$$

In this paper, we simply iterate over the possible range of k and determine the optimal value. Since the scaling factor k is now known, we can estimate $X(f)$ as follows:

$$|X(f)| = \frac{\left|\frac{1}{k} \cdot \hat{H}(f) - H(f)\right|}{|P(f)|}.$$

Comparing Figure 7(c) and Figure 7(d), we can see that with AGC calibration, the extracted in-air signal has a better SNR.

3) Signal Power Estimation: From the above step, we have extracted the in-air signal from the CFR. Next, we estimate the signal power for each frequency bin. According to the user manual of DW1000, the power of every frequency bin can be

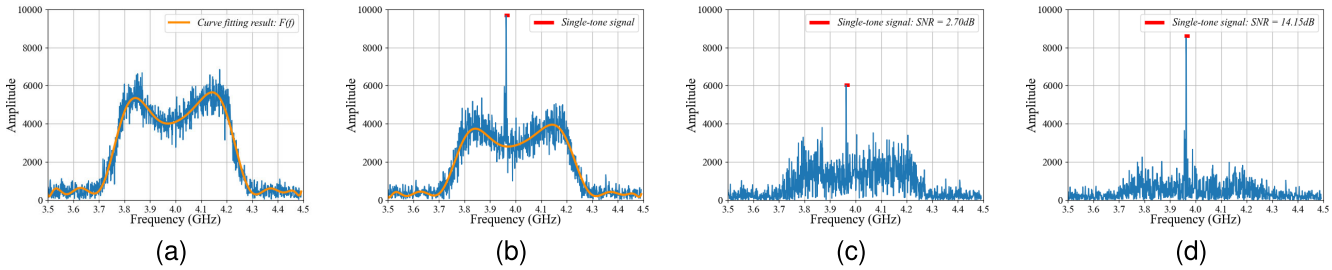

Fig. 7. CFRs with and without external signals. (a) CFR without interference. (b) CFR with interference. (c) Without AGC calibration. (d) With AGC calibration.

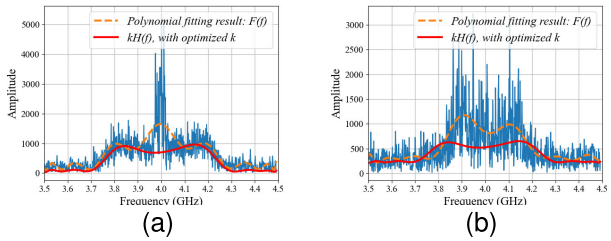

Fig. 8. CFRs for 50MHz and 300MHz signal. (a) 50MHz signal. (b) 300MHz signal.

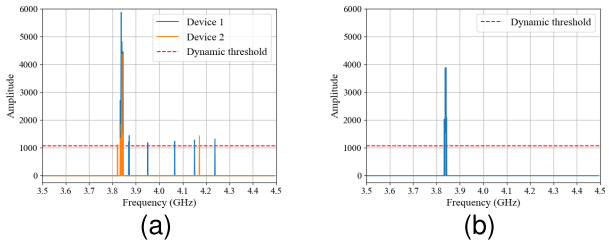

Fig. 9. Spurious frequency response. (a) CFRs from device 1 and device 2. (b) Intersections of device 1 and device 2.

calculated using the following equation:

$$Power_{Rx}(f) = 10 \times \log_{10}\left(\frac{A_f^2}{N^2}\right) - C \text{ dBm}. \quad (5)$$

Here, A_f is the amplitude of frequency f in $X(f)$ and N is the number of preamble symbols involved in the accumulation process, which can be read from PACC register. C is a constant for calibration, which is defined as 121.74 according to the DW1000 user manual. Since AGC has amplified/attenuated the receiving signals by the scaling factor k, the Equation (5) turns to be:

$$Power_{Rx}(f) = 10 \times \log_{10}\left(\frac{A_f^2}{k^2 \cdot N^2}\right) - C \text{ dBm}.$$

Thus, we can estimate the power for each frequency bin in the CFR.

4) Channel Occupation Detection: In order to determine whether the channel is occupied, we attempt to set a dynamic threshold. We design this threshold as follows:

$$Threshold = \beta \cdot mean(|X(f)|) \cdot \frac{\sum_f |X(f)|}{max(|X(f)|)}, \quad (6)$$

where β is a coefficient. For a frequency bin, if its amplitude is larger than the threshold, we consider that the channel is occupied; other*WISE*, we consider the channel to be idle.

Besides, we observe that the UWB chips may have some spurious frequency responses. We observe that, if we feed the same stimulus to the UWB chip multiple times, the chip may return different frequency responses; if the same stimulus is fed into two chips at the same time, they may also return different results, as shown in Figure 9. A nearby transmitter is transiting at 3.84GHz, but both devices have some spurious peaks at other frequencies. This phenomenon is quite random and unpredictable. As UWB is proprietary technology, it is hard to find the root cause for this uncontrollable phenomenon. In order to address this problem, *WISE* integrates two UWB receivers in the receiving block. It is very unlikely that the spurious responses will appear at the same frequency. Thus, by taking the intersection of the CFRs from the two receivers, these spurious responses can be eliminated. By taking the intersections of Device 1 and Device 2 in Figure 9(a), the spurious responses are eliminated. The results are shown in Figure 9(b). We will show in Section VII-B. that with two receivers the false positive rates can be greatly reduced.

Through the above steps, we can determine the frequency, power and bandwidth of the in-air signal.

5) Radar Mode: As we mentioned in Section IV-C1, *WISE* senses the in-air signals within the duration of the preamble. For a 64-symbol preamble, the preamble lasts for 64μ s. However, because of the limit of SPI speed (e.g., 20Mbps at maximum), it takes almost 2ms to fetch the 1016-point CIR data from the DW1000 chips. That means that *WISE* can only perform one round of spectrum sensing in every 2ms, during which the 64μ s is the sensing time while the rest time is for SPI communication. The long SPI reading time leads to a high possibility of missing fleeting or transient signals. For example, some radar signals have only one short pulse (e.g., $1 - 100\mu$ s) every 1ms. Thus, it is difficult to detect those signals, as the pulse has a high probability to occur when the *WISE* is performing SPI communication.

To address this problem, we define a radar mode in *WISE*. As more CIR points means longer SPI communication time, in radar mode, instead of getting 1016-point CIR, we just read a portion of each CIR sample from the DW1000 chip. On one hand, in radar mode, we aim to have a high update rate and thus prefer as few CIR points as possible; on the other hand, *WISE* wants to preserve a good frequency resolution. Given the 1ns sampling interval, in order to have at least 10MHz frequency resolution, we need at least 128 CIR points for FFT operations. Hence, *WISE* retrieves 150 CIR points in radar mode (extra 22 points for rough AGC calibration as explained below). According to the user manual, DW1000 arranges the

CIR buffer so that the first path index is around 750. Thus, we will read the CIR indexing from 615 to 765, reducing the SPI communication time to around 500μ s. However, it comes at the sacrifice of information and spectral resolution.

In this mode, the procedure for in-air signal extraction in Section IV-C2 no longer works well due to poor resolution. Thus, we propose an alternative solution for in-air signal extraction and signal power estimation. We further separate the 150-point CIR into two parts. The first part contains CIR1 = CIR[615:735] and the second part contains CIR2 = CIR[735:765]. We mainly use CIR1 for signal detection and CIR2 for power estimation.

As we mentioned above, the first path index is around 750. In *WISE*, the first path refers to the wired channel between the excitation block and the receiving block, i.e., $H(f)$. Thus, the energy of CIR2 mainly corresponds to the UWB signal received via the wired channel, i.e., the $k \cdot H(f)$ term in Equation (3). As the transmission power $Power_{TX}$ is a known system parameter, we can estimate k as follows:

$$k \approx \frac{\sum_{i=735}^{765} CIR[i]^2}{Power_{TX}}.$$

Compared with CIR2, the first path is less dominate in CIR1. Thus, for signal detection, we pad zeros to CIR1 and perform 128-point FFT on CIR1 to get the CFR. We also use Equation (6) to detect the channel occupation.

Although we have reduced the SPI communication time, there is still around 500μ s interval between two detections. There are possibilities that radar pulses will appear in this time gap and results in miss detection. As radar signals are composed of a number of pulses, we can detect its existence as long as one of the pulses falls within the UWB preamble duration.

We can formulate the problem for radar detection as follows. Assume that the radar signal has a pulse lasting for r second and one pulse is transmitted every R second. We use $x(t)$ to denote the radar pulse occurring at time t. There are K pulses in total. We use $Radar(t)$ to denote the radar signal:

$$Radar(t) = \begin{cases} x(t), & R \cdot k < t < R \cdot k + r,\ k \in [0, \ldots, K-1] \\ 0, & \text{else} \end{cases} \tag{7}$$

We assume that the UWB preamble lasts for μ second. We can use a binary function to indicate whether *WISE* is sensing or not:

$$WISE(t) = \begin{cases} 1, & T \cdot m + \delta < t < T \cdot m + \delta + \mu, m \in \mathbb{Z} \\ 0, & \text{else} \end{cases} \tag{8}$$

where T is the sensing cycle of *WISE* and δ is the time offset between the *WISE* and radar cycles. When *WISE* is sensing at time t, $WISE(t) = 1$; other*WISE*, *WISE* is performing SPI communication and $WISE(t) = 0$. Note that we set $t = 0$ when the first pulse in the radar signal is transmitted, and thus in Equation (8), m could be negative.

In order to detect the radar signal, we need to gurantee that at least one of the pulses is transmitted when *WISE* is sensing, that is, we need to gurantee that for any $\delta \in [0, T]$, the following condition holds:

$$\sum_t Radar(t) \cdot WISE(t) > 0. \tag{9}$$

We need to determine the appropriate *WISE* sensing cycle T. To make things simple, we can search for a feasible T, starting from the minimum value 564μs (e.g., 64μs for sensing, 500μs for SPI communication).

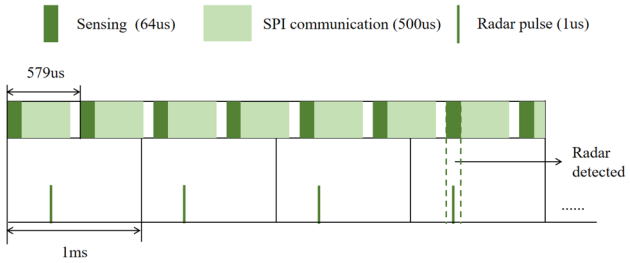

Fig. 10. Setting inter-packet interval for radar detection.

Figure 10 gives an illustrative example. Consider a typical radar signal, where $R = 1$ms, $r = 1\mu$ s, $k = 15$. Assume that the preamble of UWB packet lasts for 64μs, i.e., $\mu = 64\mu$s. When $T = 579\mu$s (e.g., 15μs idle time), Equation (9) holds for any δ. By setting the inter-packet time to 15μs, we can guarantee that *WISE* can capture at least one radar pulse. Here, we simply assume that the inter-packet interval is a constant value. In future work, we can set a variable inter-packet interval.

As we mentioned above, we reduce the SPI communication time at the sacrifice of resolution. Thus, *WISE* will switch between two modes, i.e., the normal mode and the radar mode. To avoid missing radar signals, by default, *WISE* will stay in the radar mode; it will switch to the normal mode when detecting a lasting signal, as the normal mode can provide better resolution and higher detection accuracy. By comparing the CFRs from two scans, we can determine the signal is lasting or fleeting.

V. *WISE* for Traffic Classification

In this section we design a new application of *WISE* to illustrate how the *WISE* can be used after it has captured the spectrum usage information. We enable *WISE* to classify encrypted Internet traffic based on spectrum usage patterns. With this application, *WISE* can be used in QoS improvement and malware detection.

Here, we will show how to classify the traffic with the example of Wi-Fi signals. When users are using their smartphones to play mobile games or download files from Internet with Wi-Fi, there will be huge differences between the spectrum usage patterns of gaming and downloading, as shown in Figure 11 where horizontal axis represents time, and the vertical axis represents whether the Wi-Fi channels are being occupied ("1" indicates occupied, "0" indicates idle).

We enable *WISE* to classify three categories of applications including watching a video, playing games and downloading files by following steps:

- Spectrum sensing. *WISE* will keep continuous spectrum sensing for over 1 minute at 2.4GHz where Wi-Fi signal

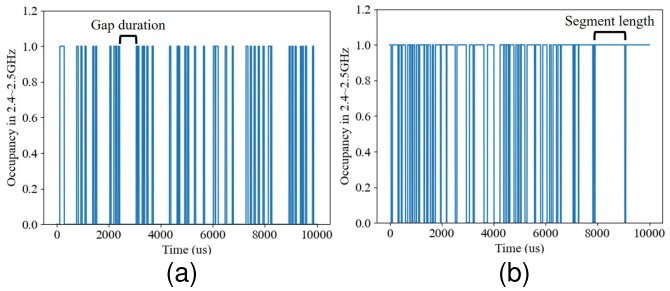

Fig. 11. Wi-Fi spectrum usage patterns in different applications. (a) Spectrum usage pattern of mobile gaming. (b) Spectrum usage pattern of file downloading.

is located. For every CFRs obtained from every 2ms continuous spectrum sensing, *WISE* will estimate the energy in the band from 2.4GHz to 2.5GHz and save the estimation results in the buffer.

- Preprocessing: We first calculate the average of the data from several consecutive frames to reduce the noise. Then we judge the occupancy of the Wi-Fi channel according to the processed channel energy. Then we take time as the X-axis and channel occupation as the Y-axis to draw the spectrum usage patterns, as shown in Figure 11. In the Y-axis, "0" means the channel is idle. "1" indicates that the channel is occupied. "Segment" in the figure represents the segment that the channel is continuously occupied, and "Gap" represents the segment that the channel is continuously idle.
- Feature extraction: From the different usage patterns of Wi-Fi signal, we can easily tell between gaming and downloading, since the gaming pattern has lower duty-cycle, lager gap duration and smaller segment length as shown in Figure 11. Therefore, we extract seven features including the maximum/average/variance of the segment length and gap duration, and duty cycle of the spectrum usage pattern.
- Classification: Considering the extremely limited computing resources on low-cost devices, we decide to use k-nearest neighbors (KNN) algorithm to classify different applications from those features.

For now, we design *WISE* to classify four states of Wi-Fi channels. In the future, *WISE* can be used in more complex scenarios by combining with other intelligent algorithms like algorithms in [27], [28], and [29].

VI. Implementation

A. Prototype

We build a prototype of *WISE* with three DW1000 UWB chips (EVK1000 [30]), one for the excitation block and two for the receiving block. DW1000 supports 6 RF bands from 3.5GHz to 6.5GHz and the maximum receiver bandwidth is about 900MHz. For expanding the frequency range of DW1000, we add a Mini-Circuits ZX05-42MHz-S+ mixer to the sensing block and use USRP N210 as the LO source. In this work, the main goal is to demonstrate the feasibility of UWB chips for spectrum sensing, and thus we use a laptop to serve as the controller, which can be easily replaced by Raspberry Pi or MCU. Two Cheetah SPI host adapters serve

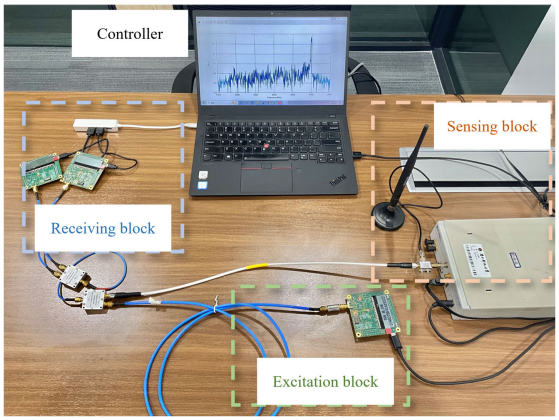

Fig. 12. *WISE* prototype.

to connect the EVK1000 to the USB port of the laptop, which can provide 20Mbps SPI speed. The communication between the controller and DW1000 is performed via the SPI interface. Figure 12 gives a picture of the prototype we have built.

We control the EVK1000s by the *decadrivers* provided by Decawave. For the excitation block, we adopt the following configuration: 64-symbol preamble, 64MHz PRF, 6.8MHz data rate and 1 byte payload. We use *Transmit Power Control* register to dynamically control the TX gain. We control the *System Control* register to trigger packet transmission. The receiver will read either 150 or 1016 points CIR from the *ACCMEM* register, depending on the working mode of *WISE*.

On the controller, we use python to process the CIR data. We use *fft* and *ifft* functions from *scipy* for transformation between CIR and CFR, and use *polyfit* function from *numpy* for 16-order polynomial curve fitting. As most processing procedures are simple operations, the processing latency is low. The controller will decide the TX gain and working mode for the next detection based on the processing result.

B. Testbed

We evaluate the performance of *WISE* through a group of experiments. We test *WISE* under two different settings. In the first setting, we use a signal generator to generate controlled signals. Here we use Keysight M8190A arbitrary waveform generator [31]. We use SystemVue [32], a software produced by Keysight, to configure the parameter of signals and download the designated signals into M8190A. Then, the output from M8190A is connected to the Keysight E8267D PSG Vector Signal Generator [33], which will up-convert the baseband signal to any frequency between 250kHz and 20GHz. Finally, the signals with designated frequency, bandwidth, and power are generated. In the second setting, we use *WISE* to monitor on-going 5G signal in the air. We use a XIAOMI 12 pro 5G to download a large file from the Internet and use Speedtest to get the connection information, including channel frequency, signal bandwidth and power. We put the *WISE* prototype 2 meters away from the 5G smartphone, as shown in Figure 18. The information from Speedtest serves as the ground truth.

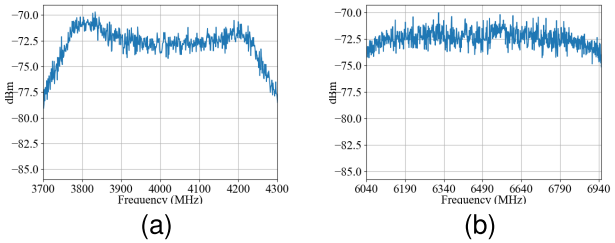

Fig. 13. Frequency response of channel 2 and channel 7. (a) Channel 2. (b) Channel 7.

VII. Evaluation

In this section, we present the evaluation results of *WISE*. We mainly consider the following evaluation metrics:

- False Negative Rate (FNR): The proportion of occupied frequencies that *WISE* incorrectly reports as empty.
- False Positive Rate (FPR): The proportion of empty frequencies that *WISE* incorrectly reports as occupied.
- True Positive Rate (TPR): the proportion of occupied frequencies that *WISE* correctly reports as occupied.

A. Frequency Response

We measure the frequency response of *WISE*. DW1000 supports 6 channels, where channel 1, 2, 3 and 5 have 499.2MHz bandwidth, while channel 4 and 7 support above 1GHz bandwidth (according to the datasheet, the maximum receiver bandwidth is approximately 900 MHz). Here, we choose to measure the frequency response of channel 2 and 7, as there are no ambient signals at these two bands and thus we can get accurate frequency responses. We believe that the measurement results are representative of other channels. Channel 2 covers from 3.774GHz to 4.243GHz, and channel 7 covers from 5.980GHz to 6.999GHz. In this experiment, to measure the frequency response, we use the signal generator to generate a 1MHz BPSK signal at -70dBm. We sweep its frequency from 3.7GHz to 4.3GHz when measuring the frequency response of channel 2, and sweep the frequency from 6.04GHz to 6.94GHz when measuring channel 7. Both channels are measured with 1MHz frequency resolution. In order to avoid signal attenuation over wireless channels, in this experiment, the output from the signal generator is connected to *WISE* input port via a wire.

Results are shown in Figure 13. The actual bandwidth of channel 2 is approximately 400MHz, covering from 3.8GHz$-$4.2GHz. The best frequency range for channel 7 to detect signals is from 6.14GHz to 6.84GHz. Generally speaking, *WISE* has a flat frequency response; for channel 2, the available bandwidth is about 400MHz, while for channel 7, the available bandwidth is about $700-900$MHz.

B. Different Modulation Schemes

To avoid interference from ambient cellular or ISM band signal, we configure the working channel of DW1000 to be channel 2, ranging from 3.774 GHz to 4.243 GHz. We check with a spectrum analyzer that the band is originally idle. We test with three different kinds of modulation schemes, i.e., BPSK, QAM and OFDM. The signal bandwidth is 10MHz.

TABLE II
Sum of False Positive Rate and False Negative Rate for *WISE* and State-of-the-Art Prior Work

Modulation	Bigband	SweepSense	S^3	*WISE*
BPSK	14.38%	4.88%	0.00%	0.28%
64QAM				0.35%
OFDM				0.35%

We tune the center of signal frequency from 3.8 GHz to 4.2 GHz, at 20MHz interval, which results in 21 channels. At each channel, we transmit the designated signals for 400 times. At a specific frequency f, if the signal is missed, we count it as a false negative event; if other frequencies (f') are identified to be occupied, we count it as a false positive event at f'.

Results are shown in Figure 14. In Figure 14(a), we show FPR and FNR for different frequency bands. In each frequency, we will transmit the signals for 1200 times in total (400 times for each modulation scheme), and obtain the FNR by dividing the count of false negative events by total transmission times. We can obtain FPR similarly. In all cases, the FPR and FNR are lower than 1%, and for more than 75% of the bands, the FPR/FNR is lower than 0.1%/0.3%, respectively. We note that FNR is generally higher than FPR. This is because FN event happens when a signal is missed at frequency f, while FP event can happen at any frequency other than f. In Figure 14(b) and Figure 14(c), the horizontal axis represents different modulations. Each designated signal will be transmitted for 8400 times in total (400 times for each channel). Figure 14(b) and Figure 14(c) show that using two receivers can reduce FPR by 10 times, which is a great improvement compared to the single receiver. We can see that *WISE* has indistinguishable performance for different modulation schemes, as the difference of FNR and FPR between different modulation schemes is less than 0.1% when two receivers have been used.

Also, we compare the performance of *WISE* with different spectrum sensing methods, including Sweep-Sense [5], S^3 [10], and Big-band [7]. Results are as shown in Table II. From Table II, we learn that, *WISE* has similar performance to S^3. However, the spike-train of filters in S^3 is customized hardware, which is not ready for mass production. Nevertheless, *WISE* is built with commercial devices.

C. Different Levels of Spectrum Occupancy

In this Section, we evaluate the performance of *WISE* under different levels of spectrum occupancy. We divide the whole band (i.e., 3.8 GHz-4.2 GHz) into 20 channels, each with 20 MHz bandwidth. In SystemVue, we emulate 20 transmitters, one at each band, each with 20MHz bandwidth. We change the level of spectrum occupancy by switching the transmitters on and off. We vary the spectrum occupancy from 10% to 90%. Under each level of spectrum occupancy, we randomly select six combinations of transmitters. For example, if 10% of the spectrum is busy, which corresponds to 2 active transmitters, we will randomly select six combinations out of the total 190 possible combinations. For each spectrum occupancy and transmitter combination, we will transmit

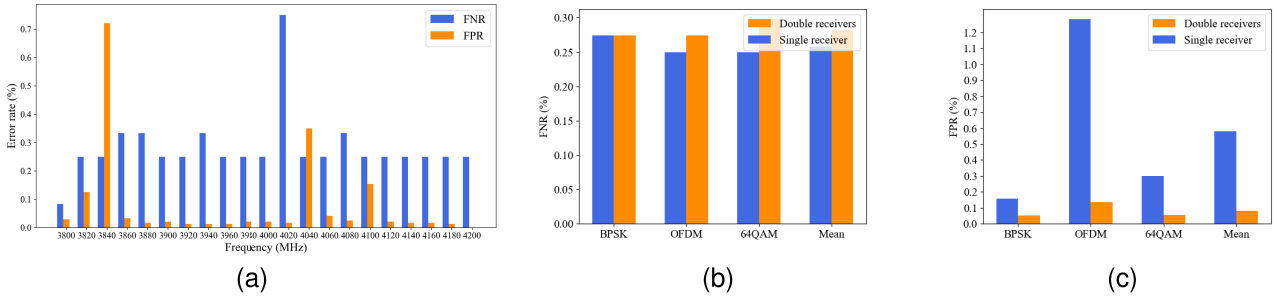

Fig. 14. *WISE* performance under different frequencies and modulation schemes. (a) The performance at different frequencies. (b) FNR of modulation schemes. (c) FPR of modulation schemes.

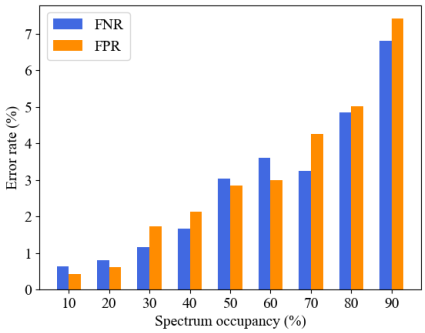

Fig. 15. CFRs under different levels of spectrum occupancy.

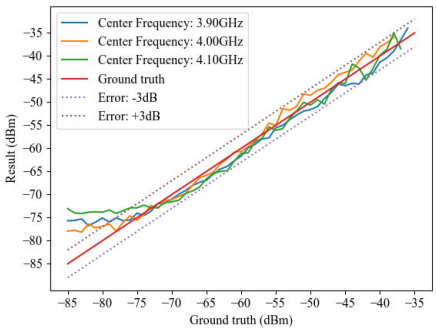

Fig. 16. The performance of power estimation.

signals for 400 times. If the signal in the positive band is missed, we count it as a false negative event; if other empty bands are identified to be occupied, we count those events as false positive events. Then we can obtain the FNR/FPR by dividing the count of false negative events/false positive events with total 400 transmissions in each spectrum occupancy level.

Results are shown in Figure 15. We can see that *WISE* has good performance at different levels of spectrum occupancy. When the spectrum occupancy is below 40%, the FPR/FNR is less than 2%; when the level of spectrum occupancy is below 80%, the FNR and FPR are less than 5%. However, when the level of spectrum occupancy increases, the performance of *WISE* will get worse. When spectrum occupancy is up to 90%, the FNR and FPR will be around 7%. By comparing the CFR under different levels of spectrum occupancy, we infer that, when the spectrum is densely occupied, the high FNR/FPR is caused by the low power spectral density. As the signal is generated by M8190A, given the limited transmission power, the power spectrum density decreases when the bandwidth increases. This is the problem of the signal generator, but not *WISE*. We believe that the performance of *WISE* may not degrade when the spectrum is occupied by independent transmitters.

TABLE III
PERFORMANCE ON RADAR DETECTION

Radar type	Pulse width(us)	PRR length(ms)	Burst	TPR	FPR
1	2	1000	40	60%	0.5%
2	20	1000	20	98.6%	0.6%
3	4	1000	24	93.4%	0.8%
4	20	1000	8	85%	0.3%
5	75	1000	24	99%	0.8%

D. Power Estimation

From the frequency response curve, we notice that the response are diverse at different frequencies. To avoid distortion in power estimation, we have calibrated the result according to the frequency response curve. In this experiment, to see whether the calibration works, we test with signals at different frequencies. We use the signal generator to generate a 50MHz BPSK signal at 3.9GHz, 4.0GHz, 4.1GHz and adjust its power from -85dBm to -35dBm, where the UWB TX power is set to -86.3dBm/MHz. Note that in Section IV-B, the bandwidth of the testing signal is 10MHz, while the bandwidth is 50MHz in this experiment.

Results are shown in Figure 16. *WISE* can estimate the signal power within $\pm$3dB error in its working range. Here we find that although the signal power exceeds -44dBm, it is still able to detect the signal. This is because we use a 50MHz signal, and its power density is lower than a 10MHz signal given the same total power. We can see that *WISE* has good accuracy in estimating signal power.

E. Radar Detection

We evaluate the performance of *WISE* in detecting radar signals. According to DeepRadar [34], we test with different types of radar signals in the CBRS band. We change the parameters of radar signals, including the pulse repetition rate (PRR), pulse width and burst length according to DeepRadar [34]. In Table III, we give the typical configurations for five types of radar signals. As we present in Section IV-C5, as long as one pulse in the burst is detected, we consider it as a radar detection event and count it as a true positive event; if no pulse in a burst is identified, we will count it as false positive events. Then we can calculate the TPR and FPR.

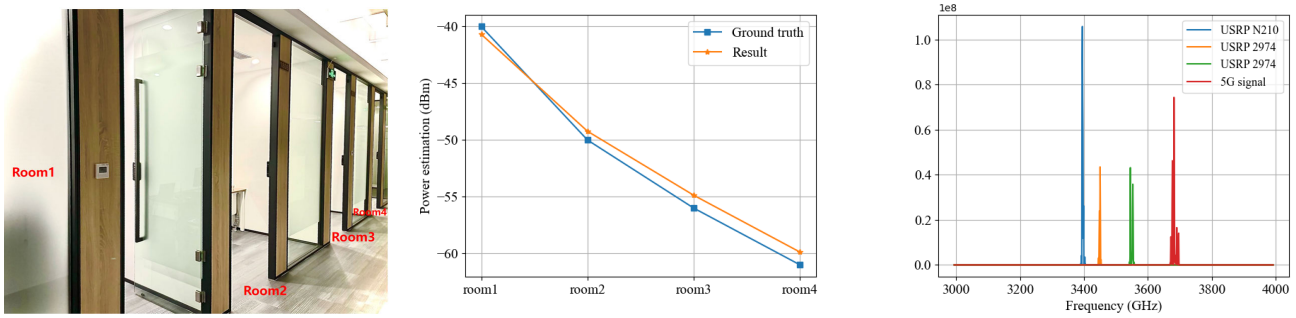

Fig. 17. Performance in complex environment. (a) Complex environment. (b) The performance in complex environment. (c) The performance of detecting concurrent transmissions.

From the results, we can see that the pulse width and burst length are deterministic factors for signal detection. A shorter burst length indicates fewer radar pulses, which increases the probability of miss detection. This is evident by comparing the performance of Radar Type 2 and Radar Type 4. When the radar signal (Type 2) lasts for over 20ms, *WISE* can have enough time to detect at least one pulse, and the TPR can reach 98.6%. However, when the pulse width is shorter than 2μ s (Type 1), even if the radar pulse occurs at the same time as the UWB preamble, we still have a high probability of miss detection. That is because DW1000 will accumulate the cross-correlation results of 64 symbols until saturation, the radar pulse whose duration is 2μ s can be buried in those 64μ s preamble symbols, resulting in a low SNR and thus miss detection. Another possible reason for miss detection is that the pulse may occur after the accumulation stops. The accumulator will stop accumulation either when the accumulator saturates or it grows quickly. The results in Table III show that *WISE* has good performance in detecting the majority of radar signals.

F. Complex Environment

In order to test the performance in more challenging setups, we evaluate *WISE* in a through-the-wall scenario and with the presence of multiple active radios. For the through-the-wall experiment, the test environment is shown in Figure 17(a). In Room 1, we set a USRP N210 as the signal source which continuously transmits OFDM signal with 10 MHz bandwidth. Then we put *WISE* in different rooms to detect this signal and estimate its power. In order to obtain the ground truth, we use the RS FSH Handheld spectrum analyzer (9KHz-8GHz) [35] to estimate the signal power in the same place as *WISE* device. In each room, *WISE* conducts power measurement 400 times, and then we average the results of 400 measurements. Results are shown in Figure 17(b). Although the signal has penetrated through three walls from Room 1 to Room 4, *WISE* can still detect its presence and estimate its power with less than 1 dB error.

We also test the performance of *WISE* to detect concurrent transmissions of multiple radios. In this experiment, we use one USRP N210 and two TX channels of USRP 2974 to send OFDM signal with 10MHz bandwidth at center frequencies of 3.4 GHz (USRP N210), 3.45 GHz (channel 0 of USRP 2974), 3.55 GHz (channel 1 of USRP 2974), concurrently. At the same time, we use a 5G base station emulator (5GS-W500 from V3 technology) to transmit 5G signals at NR77/78 band (3.6 $\sim$ 3.7 GHz). Then we use *WISE* to detect these four signals. The result is shown in Figure 17(c). We can see that *WISE* has successfully captured the signal at each corresponding frequency. Thus, *WISE* can work reliably when there are concurrent transmissions of multiple radios in the environment.

G. 5G Signal Detection

To evaluate the performance of *WISE* in the field, we attempt to detect in-air 5G signal with *WISE*. As shown in Figure 18(a), we put a Xiaomi 12 Pro 5G smartphone on a table which is about 2m from the *WISE* prototype. The smartphone is downloading a large file from the Internet. The connection information, i.e., the 5G band and signal power, is obtained from Speedtest. The details are also shown in Figure 18(b). We can see that the smartphone is working in NR77/78 band and the signal power is -72dBm.

The spectrum sensing result from *WISE* is shown in Figure 18(c). From the results, we can see that 3.5GHz $\sim$ 3.6GHz is occupied, which corresponds to the NR77/78 band. The power estimation result is shown in Figure 18(b). At about 2.2s, we start to download the file. *WISE* estimates the signal power to be around -73dBm, which is close to the information we obtain from Speedtest.

To more comprehensively demonstrate *WISE*'s ability to detect 5G signals, we use the 5G base station emulator, 5GS-W500 from V3 technology, to transmit 5G signals, and deploy *WISE* to detect 5G signals at different distances from the source. At each distance, *WISE* will estimate the signal power 400 times. In order to obtain the ground truth, we use the RS FSH Handheld spectrum analyzer (9KHz-8GHz) to estimate the signal power by taking the average value of multiple measurements at each distance. Then we average the results of 400 measurements from *WISE* and compare them with the ground truth. As the 5G signal is not a constant wave, where the active RUs keep changing, it results in the variation of the signal power, which is shown in Figure 18(d). Thus, it is hard to get accurate measurements of instantaneous 5G signal power. By averaging over a time period, the power estimation from *WISE* deviates less than 3dB from the spectrum analyzer, which is shown in Figure 18(e).

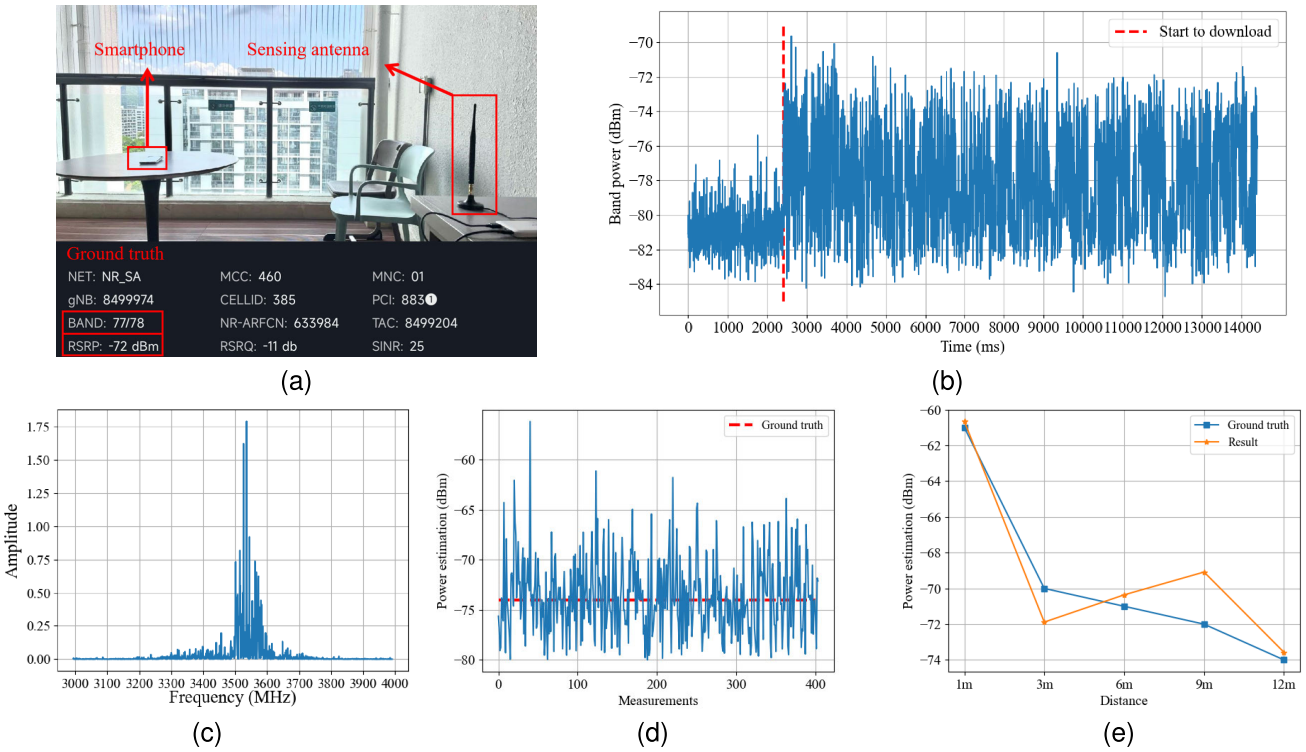

Fig. 18. Performance of detecting 5G signals. (a) Testing environment and ground truth. (b) Energy change on NR77/78 band. (c) The spectrum of 5G signal. (d) Power estimation of 5G signals at distance of 12m. (e) Power estimation at different distances.

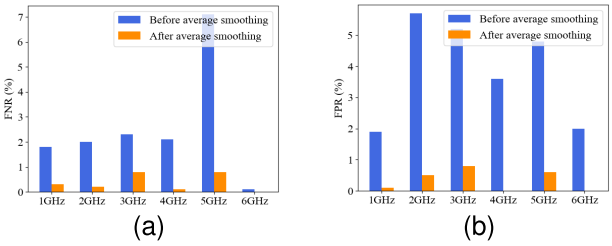

Fig. 19. Error rate with addition of mixer. (a) FNR. (b) FPR.

From these results, we can conclude that *WISE* can reliably detect 5G signal and accurately estimate its power, which implies that *WISE* can help with strategic spectrum planning and allocations. Thanks to its low cost and wideband nature, it is feasible to deploy *WISE* at a city scale for fine-grained spectrum measurement.

H. Frequency Extending

In other to evaluate the performance of *WISE* outside the default UWB channels, we use the testbed to generate OFDM signals with 10MHz bandwidth and tune the center of signal frequency from 1 GHz to 6 GHz, at 1GHz interval. Then we mix those OFDM signals into the UWB bands, and evaluate *WISE*'s ability to detect those signals. At each frequency, we transmit the designated signals for 1000 times. Then we calculate the FPR and FNR, as defined in Section VII-B.

The results are shown in Figure 19. With the mixer, the performance of detecting signals is getting worse compared with the results in Section VII-B. This is because, with the addition of mixers, the system noise increases. For example, in the case of 5GHz signal detection, we set the LO frequency to 1.4GHz so that we can up-convert 5GHz signal to 6.4GHz, then we detect this signal by setting UWB channel to Channel 7 which covers from 5.980GHz to 6.999GHz. As 1.4GHz LO signal can generate a LO resonance at 7GHz, which is very close to the UWB frequency range, it could potentially bury some signals and lead to a higher FNR. In order to reduce noise, we compute the average of the data from several consecutive frames. In this way, the noise is well suppressed and the error rate is reduced to less than 1% as shown in Figure 19. The results indicate that, the addition of the mixer enables *WISE* to detect a wider range of signals from 1GHz to 6GHz with accuracies of over 99%.

I. Ambient Signal Detection

In this section, we attempt to evaluate *WISE*'s performance of detecting ambient signals which are outside the UWB frequency range, such as 4G signals and WIFI signals. For that, we use *WISE* to conduct continuous spectrum sensing for 30 seconds in frequency range from 2GHz to 3GHz which is allocated for 4G service and WIFI service, and range from 500MHz to 1.5GHz which is allocated for digital television service (700MHz $\sim$ 800MHz) and 3G/4G LTE service (850MHz $\sim$ 1GHz). We design a trace process that retain the maximum power level from the continuous spectrum sensing results for *WISE*. Then, we use the RS FSH Handheld spectrum analyzer to sense the same bands for 30 seconds, and use its Maximum Trace result as ground truth.

The observation results are shown in Figure 20. Compared with ground truth, *WISE* accurately captures the corresponding signal on each frequency band, though there are some differences in power level compared with the spectrum analyzer,

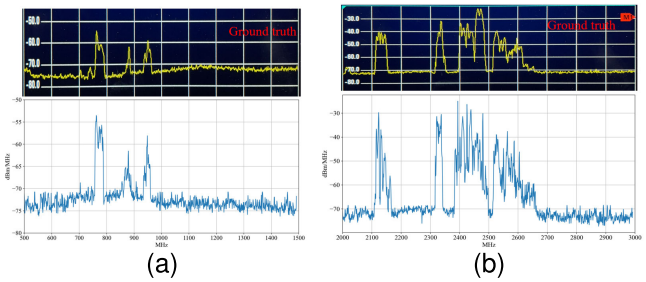

Fig. 20. Spectrum result of 500MHz to 1GHz and 2GHz to 3GHz. (a) Spectrum result of 500MHz to 1.5GHz. (b) Spectrum result of 2GHz to 3GHz.

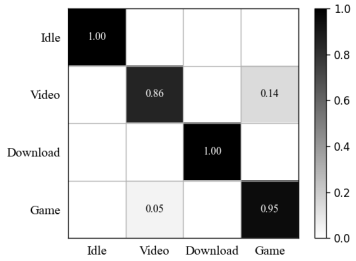

Fig. 21. Classification accuracy of *WISE*.

which is possibly due to the time offset between the spectrum analyzer and *WISE*. The results show that, *WISE* can be used to observe the ambient signals, even if they appear outside the limited UWB frequency range.

J. Traffic Classification

In other to show *WISE*'s ability to classifying the encrypted Internet traffic, we use *WISE* to classify four categories of applications including watching a video, playing games, file downloading and idle state based on the spectrum usage patterns of Wi-Fi channels. We test with an iPhone 12 mobile phone which is connected to the Internet via Wi-Fi. The smartphone is involved in four states, including watching videos at different resolutions (e.g. 480P, 720P, 1080P), playing mobile games, downloading, and the idle state. In each state, *WISE* will keep a continuous spectrum sensing in Wi-Fi channel and collect 140,000 pairs of CIR data for training, spanning over 5 minutes, and we also collect another 140,000 pairs of CIR data for testing. This data collection process spans 4 days, with training data collection in the first two days and testing data collection in the last two days. Considering users' smartphone usage habits, we define 20000 consecutive pairs of CIR as one sample, which lasts for approximately 43 seconds. In this way, there are 7 samples for training and another 7 samples for testing in each state. This results in a total of 42 samples for training and an additional 42 samples for testing. Finally, we use the confusion matrix to illustrate *WISE*'s capacity to classify the encrypted internet traffic.

The results are shown in Figure 21, and it shows that *WISE* can accurately distinguish whether the current device is in downloading or idle state. However, it can be challenging for *WISE* to differentiate between playing games and watching videos. This is because smartphones continuously cache video segments during playback, leading to a usage pattern similar to playing games. Nevertheless, *WISE* can still achieve a mean accuracy of 95.25% in classifying these different states. Furthermore, *WISE* will be able to distinguish more types of applications by employing more advanced learning algorithms, and it has the potential to be used in QoS improvement and malware detection.

VIII. Related Works

A. UWB Sensing

In recent years, UWB technology has become popular in both academics and industry. Thanks to its low cost and wideband nature, UWB has good performance in localization and sensing. On one hand, UWB technology has been used in indoor positioning [36], [37], [38], [39], [40], [41]. As the positioning accuracy of UWB can be of centimeter level, it can be used to track a writing trajectory of a pen [39], track the firefighters in buildings from outside [36], and track a ball's 3D trajectory for sports analytics [37]. On the other hand, UWB has also been used for pervasive RF sensing [42], [43], [44], [45], [46], [47], [48], [49]. Octopus [45], a UWB MIMO sensing platform, has superior performance in passive localization, vibration sensing, and human/object imaging. Similarly, MoRe-Fi [43], [44], another UWB radar, employs deep contrastive learning to detect vital signs (particularly heartbeat and breath) despite the interference caused by body movements; SiWa [46] uses the UWB signal to identify the internal structure of the wall without breaking it; LiquID [49] can distinguish different types of liquids using the time-of-flight of signals to calculate the dielectric constant of liquids. In short, UWB has great potential in RF sensing.

UWB technology has also been integrated into many commercial products, such as smartphones (e.g., iPhone 14/15, Galaxy Note 20 Ultra) and IoT devices (e.g., Air tag). We expect that UWB devices will be pervasive in daily life. We envision that one day, these UWB devices are not only used for positioning or sensing, but also integrated with *WISE* for spectrum sensing. Thus, these smartphone and IoT devices may become spectrum sensors for city-level spectrum sensing.

B. Wideband Spectrum Sensing

Spectrum sensing is important for dynamic spectrum allocation. The authors in [3], [18], [20], and [50] have built a sensor for large-scale spectrum monitoring. The spectrum sensor is built upon the low-cost commercial off-the-shelf (COTS) platform (i.e., RTL-SDR USB Dongle [3]). The total cost per sensor device is below $100. However, those low-cost spectrum sensors have narrow bandwidth (e.g., 2MHz for RTL-SDR USB Dongle, 20MHz for WiFi). In order to cover a wide spectrum, they need to hop over different bands, which leads to poor time resolution. According to the Nyquist sampling theory, wideband spectrum sensing requires high-speed ADCs, which are too expensive to be widely affordable. To monitor a 500MHz band, a 1GHz ADC is required, which costs hundreds of dollars. Recent research focuses on wideband spectrum sensing using narrowband devices with signal processing techniques (e.g., sparse Fourier transform) [7], [8], [9] or some intelligent scanning algorithms [4], [5], [6], [51]. BigBand [7] uses the sparse Fourier transform to

sense a wide bandwidth (e.g., 900MHz), when the spectrum is sparse or the changes of the spectrum are sparse. Due to the unprecedented number of wireless devices, the assumption that the spectrum is sparsely occupied may no longer hold. SpecInsight [4] can sense multi-GHz bands with 40MHz USRPs. Instead of sequentially scanning the whole band, SpecInsight will sense the channels that are likely to be active with high priority. Based on signal usage patterns, the authors use machine learning to predict spectrum occupancy. It works for known signal patterns, but for unpredictable signals, the performance of SpecInsight will degrade. SweepSense [5] can sweep the multi-GHz bands within several milliseconds by tuning the center frequency of USRP quickly. However, SweepSense also has poor performance when the spectrum is not sparse [10]. S^3 designs spike-train like filters based on MEMS acoustic resonators, which can sparsity the spectrum and enable sub-Nyquist rate sampling [10]. S^3 can sense over 500MHz bandwidth at once with two low-speed ADCs. However, the spike-train filters are customized, which are not ready for mass production. The previous work in [52] realizes wideband spectrum sensing based on UWB. However, limited by the UWB frequency, it fails to detect 2.4G Wi-Fi and LTE signals.

In summary, the current wideband spectrum monitoring techniques have clear limitations. In our work, we enable wideband spectrum monitoring with low-cost, commercial off-the-shelf UWB chips. Different from existing low-cost spectrum sensors, *WISE* not only can sense a wide spectrum, but also has high accuracy, good time resolution, and wide dynamic range. It can also detect fleeting signals like radar.

IX. Discussion

Here, we discuss the remaining issues in *WISE* and present possible countermeasures. On the one hand, in the current *WISE* design, the signal power that *WISE* can detect depends on the TX power of the excitation block. If the TX power is low, the high-power external signal may lead to failure in UWB packet detection and thus no valid CIR; if the TX power is high, the external signal will be buried in the UWB signals and leads to poor signal quality. From Section IV-B, *WISE* can sense signals ranging from -85dBm/MHz to -34dBm/MHz, which is limited by the 30dB range of DW1000 transmission gain. In order to further extend this range, we can replace the current 15dB attenuator with a digital variable attenuator. *WISE* can dynamically adjust the attenuator so that we can extract the in-air signals with good quality. Furthermore, we can add a power amplifier between the receiving antenna and the combiner to amplify external signals, so as to improve the sensitivity of *WISE* and enable it to sense weak signals.

On the other hand, as spectrum sensing plays a crucial role in spectrum management, signal propagation research, and interference source localization, it can help network companies in QoS improvement, base station deployment and maintenance. However, it incurs high deployment cost use some dedicated hardware for large scale spectrum sensing. A more low-cost way is to implement *WISE* in some commercial products such as smartphones (e.g., iPhone 14/15 [11], [12]) and IoT devices (e.g., Air tag [15]). It would be our future work to try to use these daily commercial products for spectrum sensing. For example, in a smart home, we can use a smartphone as the transmitter, and another two UWB IoT devices as the receivers, so they work collaboratively as a spectrum sensor. Network companies can encourage mobile users to participate in spectrum sensing in a crowd-sourcing manner by offering discounts on phone credit or mobile data plans. Additionally, due to *WISE*'s low duty cycle (e.g.working for 64μ s every 2ms in normal mode) and low transmit power (e.g.-104.3dBm/MHz), the energy consumption of *WISE* is quite low. So network companies can partner with the government to integrate *WISE* into low-power public IoT devices such as smart streetlights or road signs, enabling city-wide spectrum monitoring.

X. Conclusion

In this paper, we present how we transform UWB chipsets into a spectrum sensor. We introduce the design of *WISE*, a lost-cost wideband spectrum sensing unit, which is built with the commercial off-the-shelf UWB chip, DW1000. *WISE* can sense up to 900MHz bandwidth without using expensive high-speed ADCs. *WISE* exploits the channel impulse response to obtain the spectrum occupancy information. We implement *WISE* and extensively evaluate its performance. Results show that *WISE* can accurately detect spectrum occupancy and estimate the signal power/bandwidth with high precision. *WISE* can also detect fleeting radar signals. We also demonstrate *WISE* with a field test, where *WISE* can accurately detect 5G signals and estimate 5G signal power. We believe that *WISE* brings a new paradigm for spectrum sensing. As UWB chipsets are becoming popular on smartphones and IoT devices, we expect that in the future, these commodity devices may participate in city-level spectrum sensing.

References

[1] (2020). *FCC Opens 6 GHz Band to Wi-Fi and Other Unlicensed Uses*. [Online]. Available: https://www.fcc.gov/document/fcc-opens-6-ghz-band-wi-fi-and-other-unlicensed-uses-0

[2] (2020). *3.5 GHz Band Overview*. [Online]. Available: https://www.fcc.gov/35-ghz-band-overview

[3] D. Pfammatter, D. Giustiniano, and V. Lenders, "A software-defined sensor architecture for large-scale wideband spectrum monitoring," in *Proc. 14th Int. Conf. Inf. Process. Sensor Netw.*, Apr. 2015, pp. 71–82.

[4] L. Shi, P. Bahl, and D. Katabi, "Beyond sensing: Multi-GHz realtime spectrum analytics," in *Proc. NSDI*, 2015, pp. 159–172.

[5] Y. Guddeti, R. Subbaraman, M. Khazraee, A. Schulman, and D. Bharadia, "Sweepsense: Sensing 5 GHz in 5 milliseconds with low-cost radios," in *Proc. NSDI*, 2019, pp. 317–330.

[6] S. Yoon, L. E. Li, S. C. Liew, R. R. Choudhury, I. Rhee, and K. Tan, "QuickSense: Fast and energy-efficient channel sensing for dynamic spectrum access networks," in *Proc. IEEE INFOCOM*, Apr. 2013, pp. 2247–2255.

[7] H. Hassanieh, L. Shi, O. Abari, E. Hamed, and D. Katabi, "GHz-wide sensing and decoding using the sparse Fourier transform," in *Proc. IEEE Conf. Comput. Commun. (INFOCOM)*, Apr. 2014, pp. 2256–2264.

[8] H. Hassanieh, P. Indyk, D. Katabi, and E. Price, "Nearly optimal sparse Fourier transform," in *Proc. STOC*, May 2012, pp. 563–578.

[9] B. Ghazi, H. Hassanieh, P. Indyk, D. Katabi, E. Price, and L. Shi, "Sample-optimal average-case sparse Fourier transform in two dimensions," in *Proc. 51st Annu. Allerton Conf. Commun., Control, Comput. (Allerton)*, Oct. 2013, pp. 1258–1265.

[10] J. Guan et al., "Efficient wideband spectrum sensing using MEMS acoustic resonators," in *Proc. NSDI*, 2021, pp. 809–825.

[11] (2022). *Ultra Wideband is Available on iPhone14*. [Online]. Available: https://support.apple.com/en-hk/HT212274

[12] (2020). *Apple U1 Chip Explained: What is it and What Can it Do?* [Online]. Available: https://www.pocket-lint.com/phones/news/apple/149336

[13] (2020). *NXP Secure UWB Deployed in Samsung Galaxy Note20 Ultra*. [Online]. Available: https://media.nxp.com/news-releases/news-release-details/nxp-secure-uwb-deployed-samsung-galaxy-note20/

[14] (2021). *NXP Ultra-Wideband Technology Powers Xiaomi Mix4 Smartphone to Deliver New 'Point to Connect Smart Home Solution*. [Online]. Available: https://www.nxp.com/company/about-nxp/

[15] (2021). *Apple Airtag Arrives for $29, Uses Ultra Wideband and Does Emoji*. [Online]. Available: https://www.gsmarena.com/apple_airtag_finally_arrives_for_29_uses_ultrawideband_and_does_emoji-news-48753.php

[16] (2020). *Apple Watch Series 6 Features U1 Chip for Ultra Wideband*. [Online]. Available: https://www.macrumors.com/2020/09/15/apple-watch-series-6-u1-chip-ultra-wideband/

[17] (2021). *Samsung's Galaxy Smarttag is a $29.99 Tile Competitor*. [Online]. Available: https://www.theverge.com/2021/1/14/22227621/samsung-galaxy-smarttag-price-release-date-tile-locator

[18] T. Zhang, A. Patro, N. Leng, and S. Banerjee, "A wireless spectrum analyzer in your pocket," in *Proc. 16th Int. Workshop Mobile Comput. Syst. Appl.*, Feb. 2015, pp. 69–74.

[19] A. Nika, Z. Zhang, X. Zhou, B. Y. Zhao, and H. Zheng, "Towards commoditized real-time spectrum monitoring," in *Proc. 1st ACM workshop Hot topics wireless*, Sep. 2014, pp. 25–30.

[20] A. Nika et al., "Empirical validation of commodity spectrum monitoring," in *Proc. SenSys*, Nov. 2016, pp. 96–108.

[21] Decawave. (2017). *DW1000 User Manual*. [Online]. Available: https://www.decawave.com/sites/default/files/resources/dw1000_user_manual_2.11.pdf

[22] (2011). *IEEE Standard for Local and Metropolitan Area Networks—Part 15.4: Low-Rate Wireless Personal Area Networks (LR-WPANS)*. [Online]. Available: https://standards.ieee.org/ieee/802.15.4/5050/

[23] Decawave. (2014). *Wireless Sensor Networks and the DW1000*. [Online]. Available: https://www.decawave.com/wp-content/uploads/2018/10/APS010_DW1000-and-Wireless-Sensor-Networks_v1.1.pdf

[24] Decawave. (2015). *DW1000 Data Sheet*. [Online]. Available: https://www.decawave.com/sites/default/files/resources/dw1000-datasheet-v2.09.pdf

[25] Y. Cheng, Y. Qian, H. Homma, A. A. Fathnan, and H. Wakatsuchi, "Waveform-selective metasurface absorber with a single-patch structure and lumped nonlinear circuit for a higher-order mode," *IEEE Trans. Antennas Propag.*, vol. 71, no. 11, pp. 8677–8691, Nov. 2023.

[26] Z. K. Peng, Z. Q. Lang, and S. A. Billings, "Resonances and resonant frequencies for a class of nonlinear systems," *J. Sound Vib.*, vol. 300, nos. 3–5, pp. 993–1014, Mar. 2007.

[27] Y. Zhou, H. Shi, Y. Zhao, W. Gao, and W. Zhang, "Encrypted network traffic identification based on 2D-CNN model," in *Proc. 22nd Asia–Pacific Netw. Oper. Manage. Symp. (APNOMS)*, Sep. 2021, pp. 238–241.

[28] R. Liu and X. Yu, "A survey on encrypted traffic identification," in *Proc. Int. Conf. Cyberspace Innov. Adv. Technol.* New York, NY, USA: Association for Computing Machinery, 2021, pp. 159–163, doi: 10.1145/3444370.3444564.

[29] Q. Huang et al., "Rethinking privacy risks from wireless surveillance camera," *ACM Trans. Sensor Netw.*, vol. 19, no. 3, pp. 1–21, Aug. 2023.

[30] Decawave. (2018). *EVK1000 User Manual*. [Online]. Available: https://www.decawave.com/wp-content/uploads/2018/09/evk1000_user_manual.pdf

[31] Keysight. (2021). *Keysight M8190A Arbitrary Waveform Generator*. [Online]. Available: https://www.keysight.com/hk/en/assets/7018-02903/data-sheets/5990-7516.pdf

[32] Keysight. (2022). *PathWave System Design (SystemVue)*. [Online]. Available: https://www.keysight.com/hk/en/products/software/pathwave-design-software/pathwave-system-design-software.html

[33] Keysight. (2022). *E8267D PSG Vector Signal Generator*. [Online]. Available: https://www.keysight.com/hk/en/assets/7018-01210/data-sheets/5989-0697.pdf

[34] S. Sarkar, M. Buddhikot, A. Baset, and S. K. Kasera, "DeepRadar: A deep-learning-based environmental sensing capability sensor design for CBRS," in *Proc. 27th Annu. Int. Conf. Mobile Comput. Netw.*, Sep. 2021, pp. 56–68.

[35] (2022). *RS FSH Handheld Spectrum Analyzer*. [Online]. Available: https://www.rohde-schwarz.com/us/products/test-and-measurement/handheld/rs-fsh-handheld-spectrum-analyzer_63493-8180.html

[36] A. Dhekne et al., "TrackIO: Tracking first responders inside-out," in *Proc. NSDI*, 2019, pp. 751–764.

[37] M. Gowda et al., "Bringing IoT to sports analytics," in *Proc. NSDI*, 2017, pp. 499–513.

[38] B. Anderson, M. Shi, V. Y. F. Tan, and Y. Wang, "Mobile gait analysis using foot-mounted UWB sensors," *Proc. ACM Interact., Mobile, Wearable Ubiquitous Technol.*, vol. 3, no. 3, pp. 1–22, Sep. 2019.

[39] Y. Cao, A. Dhekne, and M. Ammar, "ITrackU: Tracking a pen-like instrument via UWB-IMU fusion," in *Proc. 19th Annu. Int. Conf. Mobile Syst., Appl., Services*, Jun. 2021, pp. 453–466.

[40] P. Corbalán, G. P. Picco, and S. Palipana, "Chorus: UWB concurrent transmissions for GPS-like passive localization of countless targets," in *Proc. 18th ACM/IEEE Int. Conf. Inf. Process. Sensor Netw. (IPSN)*, Apr. 2019, pp. 133–144.

[41] B. Großwindhager et al., "SALMA: UWB-based single-anchor localization system using multipath assistance," in *Proc. 16th ACM Conf. Embedded Networked Sensor Syst.*, Nov. 2018, pp. 132–144.

[42] Y. Ma, Y. Zeng, and V. Jain, "CarOSense: Car occupancy sensing with the ultra-wideband keyless infrastructure," *Proc. ACM Interact., Mobile, Wearable Ubiquitous Technol.*, vol. 4, no. 3, pp. 1–28, Sep. 2020.

[43] T. Zheng, Z. Chen, S. Zhang, C. Cai, and J. Luo, "MoRe-Fi: Motion-robust and fine-grained respiration monitoring via deep-learning UWB radar," in *Proc. 19th ACM Conf. Embedded Netw. Sensor Syst.*, Nov. 2021, pp. 111–124.

[44] Z. Chen, T. Zheng, C. Cai, and J. Luo, "MoVi-Fi: Motion-robust vital signs waveform recovery via deep interpreted RF sensing," in *Proc. 27th Annu. Int. Conf. Mobile Comput. Netw.*, Oct. 2021, pp. 392–405.

[45] Z. Chen, T. Zheng, and J. Luo, "Octopus: A practical and versatile wideband MIMO sensing platform," in *Proc. 27th Annu. Int. Conf. Mobile Comput. Netw.*, Oct. 2021, pp. 601–614.

[46] T. Zheng, Z. Chen, J. Luo, L. Ke, C. Zhao, and Y. Yang, "SiWa: See into walls via deep UWB radar," in *Proc. 27th Annu. Int. Conf. Mobile Comput. Netw.*, Oct. 2021, pp. 323–336.

[47] Z. Wang, Z. Chen, A. D. Singh, L. Garcia, J. Luo, and M. B. Srivastava, "UWHear: Through-wall extraction and separation of audio vibrations using wireless signals," in *Proc. 18th Conf. Embedded Networked Sensor Syst.*, Nov. 2020, pp. 1–14.

[48] M. Singh, P. Leu, A. Abdou, and S. Capkun, "UWB-ED: Distance enlargement attack detection in ultra-wideband," in *Proc. USENIX Secur.*, 2019, pp. 73–88.

[49] A. Dhekne, M. Gowda, Y. Zhao, H. Hassanieh, and R. R. Choudhury, "LiquID: A wireless liquid IDentifier," in *Proc. 16th Annu. Int. Conf. Mobile Syst., Appl., Services*, Jun. 2018, pp. 442–454.

[50] S. Rajendran et al., "Electrosense: Open and big spectrum data," *IEEE Commun. Mag.*, vol. 56, no. 1, pp. 210–217, Jan. 2018.

[51] A. Chakraborty, M. S. Rahman, H. Gupta, and S. R. Das, "SpecSense: Crowdsensing for efficient querying of spectrum occupancy," in *Proc. IEEE Conf. Comput. Commun. (INFOCOM)*, May 2017, pp. 1–9.

[52] Z. Luo et al., "WISE: Low-cost wide band spectrum sensing using UWB," in *Proc. 20th ACM Conf. Embedded Netw. Sensor Syst.*, Nov. 2022, pp. 651–666.